Supplemental Information

Enrichment of histone tail methylated lysine residues via cavitand-decorated magnetic nanoparticles for ultra-sensitive proteomics

Martina Orlandini,[1]‡ Alex Bonacini,[1]‡ Alessia Favero,[1] Andrea Secchi,[1] Laura Lazzarini,[2] Roberto Verucchi,[3] Enrico Dalcanale,[1] Alessandro Pedrini,[1] Simone Sidoli[4]* and Roberta Pinalli[1]*.

[1] Department of Chemistry, Life Sciences and Environmental Sustainability, University of Parma, 43124 Parma, and INSTM, UdR Parma, Italy.

[2] IMEM-CNR, Institute of Materials for Electronics and Magnetism, National Research Council, Parma Unit, Parco Area delle Scienze 37/A, 43124 Parma, Italy.

[3] IMEM-CNR, Institute of Materials for Electronics and Magnetism, National Research Council, Trento Unit, via alla Cascata 56/C, 38123 Trento, Italy

[4] Department of Biochemistry, Albert Einstein College of Medicine, Bronx, NY 10461, USA

‡ These two Authors contribute equally to the work

Index

1. Experimental Section

All reagents and solvents were purchased from certified commercial sources and used as received, without further purification. For the synthesis, all solvents were dried and distilled according to standard procedures known in the literature.[1]

Pan-Methyl Lysine kit was purchase from Cell Signaling Technology.

Arg-C enzyme was purchase from Promega Corporation.

Thin layer chromatography was performed using TLC Analytical Chromatography F254®, Merck.

Nuclear Magnetic Resonance. ^{1}H and ^{31}P NMR spectra were recorded on Bruker 400MHz AVANCE or Jeol 600MHz using DMSO-d_6, Acetone-d_6, CD_3OD and $CDCl_3$ as solvents. All chemical shifts (δ) were reported in parts for million (ppm) relative to proton resonances resulting from incomplete deuteration of NMR solvents. The abbreviations: s, d, t, m and sb indicated the spectrum peaks referred to: singlet, doublet, triplet, multiplet and broad singlet, respectively. The coupling constant (J) are expressed in Hz.

MS Spectrometry. ESI-MS characterization experiments were performed on a Waters ACQUITY Ultra Performance LC HO6UPS-823M with ESI source ionization (electrospray ionization) in positive modality.

Fourier transform infrared spectroscopy (FTIR). FT-IR analyses were performed using Bruker FTIR LUMOS.

Thermal Gravimetric Analysis (TGA). TGA analyses have been achieved using TGA/DSC 1 with gas controller GC10 (pure air/nitrogen), Mettler Toledo.

Transmission Electron Microscopy. TEM analyses were performed using TEM JEOL JEM-2200FS with Schottky field emission gun. Operating voltage: 80 kV, 200 kV; Point resolution: 0.183 nm (TEM) and 0.132 nm (STEM); two High Angle Annular Dark Field detectors (Z-contrast); column Omega filter. Oxford AztecEnergy EDX system with the 80 mm^2 XPLORE SDD. The samples, suspended in propanol, have been sonicated and then drop casted on ultrathin carbon Cu grids.

Zeta Potential analysis. Zeta Potential analyses were performed using Malvern Instrument, Zetasizer Ver. 7.12, using a DTS 1070 disposable cuvette.

X-ray Photoelectron Spectroscopy (XPS). XPS analyses were performed ex-situ in an Ultra High Vacuum (UHV) μ-metal chamber using Mg kα 1253.6 eV photon energy. The electron energy analyzer (VSW HSA100 hemispherical analyzer with PSP electronics) has a total energy resolution of 0.82 eV for XPS. The binding energy (BE) scale for XPS was calibrated by using the Au 4f 7/2 peak at 84.00 eV as a reference. The apparatus is not equipped with a charge compensator, thus, the photoemission from insulating material can lead to charging and BE shifts. XPS spectra were background subtracted using a Shirley background, line shape analysis was performed using Voigt functions. Typical uncertainty for the peak energy positioning is ± 0.05 eV, while the full width at half maximum (FWHM) and the area evaluation uncertainties are less than ± 5% and ± 2.5%, respectively. Material stoichiometry. i.e. atomic element percentages, have been evaluated using the relative sensitivity factors approach.

LC MS/MS

DDA raw files were searched using Proteome Discoverer software (v2.5, Thermo Scientific) using SEQUEST search engine and the bovine histone database. The search for total proteome included variable modification of mono- (KR), di- (KR) and trimethyl (K). Arg-C was specified as the digestive enzyme with up to 2 missed cleavages allowed. Mass tolerance

was set to 10 pm for precursor ions and 0.2 Da for product ions. Peptide and protein false discovery rate was set to 1%. Data were then imported into Skyline[2] for extracting the ion chromatogram.

DIA raw files were imported into the EpiProfile 2.0 software.[3] From the extracted ion chromatogram, the area under the curve was obtained and used to estimate the abundance of each peptide. In order to achieve the relative abundance of post-translational modifications (PTMs), the sum of all different modified forms of a histone peptide was considered as 100% and the area of the particular peptide was divided by the total area for that histone peptide in all of its modified forms. The relative ratio of two isobaric forms was estimated by averaging the ratio for each fragment ion with different mass between the two species.

2. Structures of lysine and methylated lysines in peptides

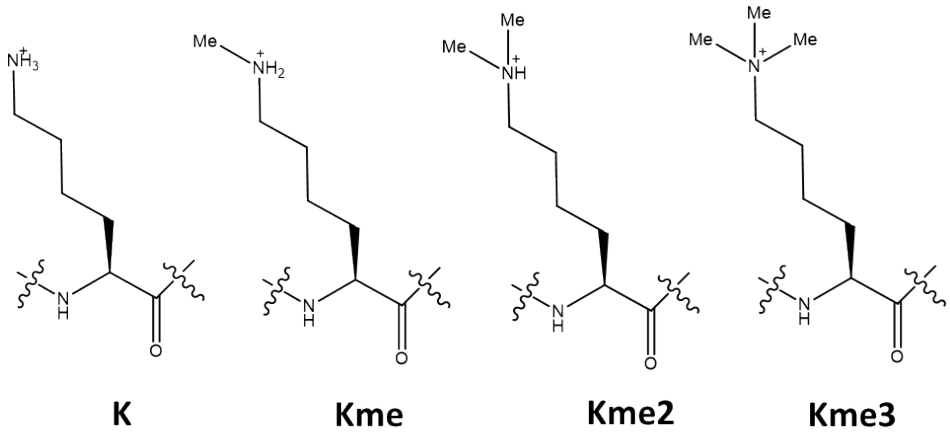

Chart S1. Structures of lysine (**K**) and methylated lysines (**Kme**, **Kme2** and **Kme3**) in peptides.

3. Cavitand Synthesis

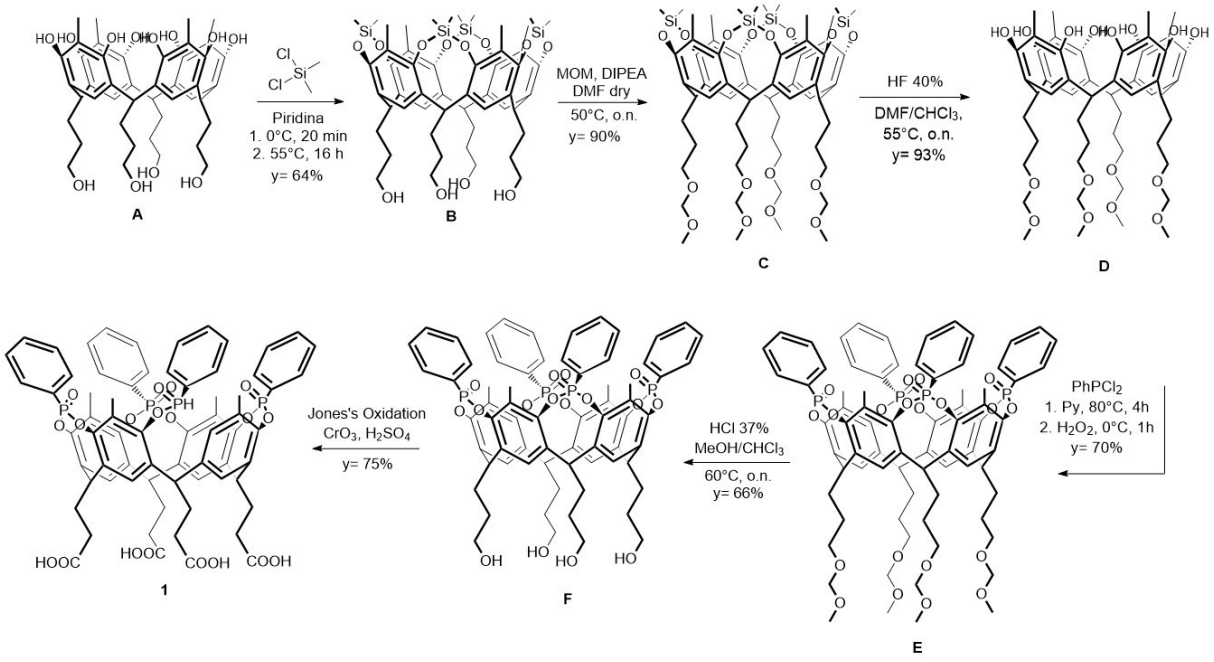

Scheme S1. Synthetic pathway for cavitand **1**.

Resorcinarene [C_3H_6OH; Me] (A)

To a solution of 2-methylresorcinol (15 g, 0.12 mol) in MeOH (90 mL), 2,3-Dihydrofuran (9.15 mL, 0.12 mol) and HCl 37% (22.5 mL) were added dropwise over 30 min at 0 °C. After the addition, the reaction mixture was stirred at 50 °C for a week. The reaction was quenched with water, filtered, dried under vacuum, and recrystallized three times from MeOH. The final product **A** was obtained as a pale yellow powder (7.9 g, 34%).**^{1}H NMR** (DMSO-d_6, 400 MHz): δ ppm = 8.66 (s, 8H, **OH**), 7.29 (s, 4H, **ArH_{down}**), 4.19 (t, 4H, -**CH**-, J = 9.80 Hz), 3.44 (m, 8H, -**CH_2**OH), 2.25 (m, 8H, CH**CH_2**-), 1.94 (s, 12H, Ar**CH_3**), 1.35 (m, 8H, -**CH_2**CH_2OH); **ESI-MS:** m/z 777.41 $[M+H]^+$.

Cavitand B

In a Schlenk reactor, under anhydrous conditions, 3.00 g (3.86 mmol) of **Res [C_3H_6OH; Me]** were dissolved in 10 mL of anhydrous pyridine. The solution was cooled down to 0 °C through an ice bath, and 8.36 mL (69.53 mmol) of $(CH_3)_2SiCl_2$ were added under magnetic stirring. The reaction mixture was kept at 0°C under magnetic stirring for about 20 minutes, and then heated to 100 °C for 3 hours. The reaction was cooled down to room temperature and the solvent was removed under high vacuum using a trap. The solid obtained was suspended in methanol, filtered, washed with methanol and finally dried. Cavitand **B** was obtained pure as a white solid, in 64% yield. **^{1}H NMR** ($CDCl_3$, 400 MHz): δ ppm = 7.47 (s, 4H, Ar**H_{down}**), 4.54 (t, 4H, -**CH**-, J = 7.9 Hz), 3.66 (bt, 8H, -**CH_2**OH), 2.45 (m, 8H, CH**CH_2**), 1.87 (s, 12H, Ar**CH_3**), 1.50-1.46 (m, 8H, -**CH_2**CH_2OH), 0.46 (s, 12H, Si**CH_{3out}**), -0.73 (s, 12H, Si**CH_{3in}**). **ESI-MS:** m/z 1002.50 $[M+H]^+$.

Cavitand C

To a solution of 3.00 g (1.00 mmol) of Cavitand **B** in 12 mL of anhydrous DMF, diisopropylethylamine (2.79 mL, 15.99 mmol) and chloromethyl methyl ether (0.79 mL, 10.5 mmol) were added under nitrogen. The suspension was stirred at 40 °C overnight. Then, the reaction was cooled down to room temperature and the solvent evaporated under reduced pressure. The obtained precipitate was suspended in water, filtered, washed with water and dried to give cavitand **C** as

light brown solid (yield 90%). **^{1}H NMR** ($CDCl_3$, 400 MHz): δ ppm = 7.17 (s, 4H, Ar**H**$_{down}$), 4.63 (s, 8H, -O**CH**$_2$O-), 4.62 (t, 4H, -**CH**-, J = 8.2 Hz), 3.58 (t, 8H, -**CH$_2$**OMOM, J = 6.3 Hz), 3.38 (s, 12H, O**CH$_3$**), 2.29 (q, 8H, CH**CH$_2$**-, J = 7.1 Hz), 1.90 (s, 12H, Ar**CH$_3$**), 1.58 (q, 8H, -**CH$_2$**CH_2OMOM, J = 7.1 Hz), 0.51 (s, 12H, Si**CH**$_{3out}$), -0.69 (s, 12H, Si**CH**$_{3in}$). **ESI-MS:** m/z 1177.53 $[M+H]^+$.

Resorcinarene [C_3H_6OMOM; Me] (D)

In a Teflon flask, to a solution of cavitand **C** (1.06 g, 0.90 mmol) in 15 mL of DMF, HF 40 % (1.00 mL, 9.62 mmol) was added. The suspension was stirred overnight at 50 °C. Then, the solvent was removed under reduced pressure and the addition of water promoted the precipitation of the product. The obtained solid was filtered, washed with water, and dried to give product **D** as a white solid in 93% yield. **^{1}H NMR** (DMSO-d_6, 400 MHz): δ ppm = 8.68 (s, 8H, Ar**OH**), 7.29 (s, 4H, Ar**H**$_{down}$), 4.53 (s, 8H, -O**CH**$_2$O-), 4.22 (t, 4H, -**CH**-, J = 7.7 Hz), 3.48 (t, 8H, -**CH$_2$**OMOM, J = 6.4 Hz), 3.33 (s, 12H, O**CH$_3$**), 2.28 (m, 8H, CH**CH$_2$**-), 1.94 (s, 12H, Ar**CH$_3$**), 1.43 (m, 8H, -**CH$_2$**CH_2OMOM). **ESI-MS:** m/z 953.51 $[M+H]^+$.

Cavitand E

To a solution of resorcinarene **D** (0.80 g, 0.84 mmol) in 16 mL of anhydrous pyridine, dichlorophenyl phosphine (0.49 mL, 3.61 mmol) was added under nitrogen atmosphere. The solution was stirred at 80 °C for 3 hours. Then, the mixture was cooled down to 0 °C with an ice bath and 2 mL of 35% aqueous H_2O_2 were added. The reaction was stirred at room temperature for 1 hour, under magnetic stirring and nitrogen flux. The crude was poured into cold water obtaining a milky solution that was kept refrigerated at 2 °C overnight. The formed precipitate was then filtered, washed with water, and dried. The obtained solid was dissolved in DMC and precipitated with hexane to give pure cavitand **E** as a white solid with a yield of 71%. **^{1}H NMR** ($CDCl_3$, 400 MHz): δ ppm = 8.13 (m, 8H, P(O)Ar**H$_o$**), 7.64 (m, 4H, P(O)Ar**H$_p$**), 7.57 (m, 8H, P(O)Ar**H$_m$**), 7.20 (s, 4H, Ar**H$_{down}$**), 4.90 (t, 4H, -**CH**-, J = 7.0 Hz), 4.84 (s, 8H, -O**CH**$_2$O-), 3.69 (t, 8H, -**CH$_2$**OMOM, J = 5.9 Hz), 3.50 (s, 12H, O**CH$_3$**), 2.46 (m, 8H, CH**CH$_2$**-), 2.29 (s, 12H, Ar**CH$_3$**), 1.70 (m, 8H, -**CH$_2$**CH_2OMOM). **^{31}P NMR** ($CDCl_3$, 162 MHz): δ ppm = 7.13 (s, P=O). **ESI-MS:** m/z 1464.36 $[M+Na]^+$.

Cavitand F

Cavitand **E** (0.86 g, 0.60 mmol) was dissolved in 6 mL of $CHCl_3$ and 12 mL of MeOH. HCl 37% (1.37 mL) was added and the solution was stirred overnight at 40 °C. The solvent was evaporated obtaining a white solid that was triturated with water, acetone and finally filtered and dried to give cavitand **F** in 86% yield. **^{1}H NMR** (MeOD-d_4, 400 MHz): δ ppm = 8.13 (m, 8H, P(O)Ar**H$_o$**), 7.76 (m, 4H, P(O)Ar**H$_p$**), 7.65 (m, 8H, P(O)Ar**H$_m$**), 7.61 (s, 4H, Ar**H$_{down}$**), 4.90 (t, 4H, -**CH**-, J = 7.3 Hz), 3.75 (t, 8H, -**CH$_2$**OH, J = 6.2 Hz), 2.60 (m, 8H, CH**CH$_2$**-), 2.28 (s, 12H, Ar**CH$_3$**), 1.66 (m, 8H, -**CH$_2$**CH_2OH). **^{31}P NMR** ($CDCl_3$, 162 MHz): δ ppm = 8.88 (s, P=O). **ESI-MS:** m/z 1297.81 $[M+K]^+$.

Tiiii-Tetraphosphonate Cavitand 1

To a solution of Cavitand **E** (0.50 g, 0.40 mmol) in 12 mL of DMF and 12 mL of acetone, CrO_3 (0.63 g, 6.34 mmol) was added under magnetic stirring. Then, H_2SO_4 (96% aqueous) was added until pH 2 was reached and the solution was stirred at room temperature for 5 hours. The dark green solution was concentrate evaporating the solvent in high vacuum trap, then acidic water was added maintaining pH 2, and the obtained suspension was centrifugated (4800 rpm, 10 minutes). The solid residue was washed many times with water till it reached a pale green color. Cavitand **1** was obtained in 55% yield. **^{1}H NMR** (MeOD-d_4, 400 MHz): δ ppm = 8.16 (m, 8H, P(O)Ar**H$_o$**), 7.82 (m, 4H, P(O)Ar**H$_p$**), 7.71 (m, 8H, P(O)Ar**H$_m$**), 7.64 (s, 4H, Ar**H$_{down}$**), 5.04 (bt, 4H, -**CH**-), 2.86 (m, 8H, -**CH$_2$**COOH), 2.45 (m, 8H, CH**CH$_2$**-), 2.18 (s, 12H, Ar**CH$_3$**). **^{31}P NMR** (MeOD-d_4, 162 MHz): δ ppm = 10.2 (s, P=O). **^{13}C NMR** (MeOD-d_4, 100 MHz): δ ppm = 175.32, 145.37,

145.26, 134.74, 134.23, 131.26, 131.15, 129.09, 128.92, 125.66, 125.23, 120.26, 36.31, 31.54, 25.84. **HR ESI-MS:** m/z calculated for $C_{68}H_{59}O_{10}P_4^-$ 1319.2556 $[M-H]^-$, found 1319.2536. **ATR-FTIR**: 2927 cm^{-1} C-H (aliphatic) and O-H; 1714 cm^{-1} C=O; 1068 cm^{-1} P=O; 900 cm^{-1} O-P-O. **TGA** (air, 25°C - 900 °C, flow rate: 20 °C/min): 0.4 % w/w loss at 29 °C; 9.5 % w/w loss at 266 °C; 20.6 % w/w loss at 441 °C; 7.6 % w/w loss at 523 °C; 16.1 % w/w loss at 574 °C; 26.7 % w/w loss at 710 °C.

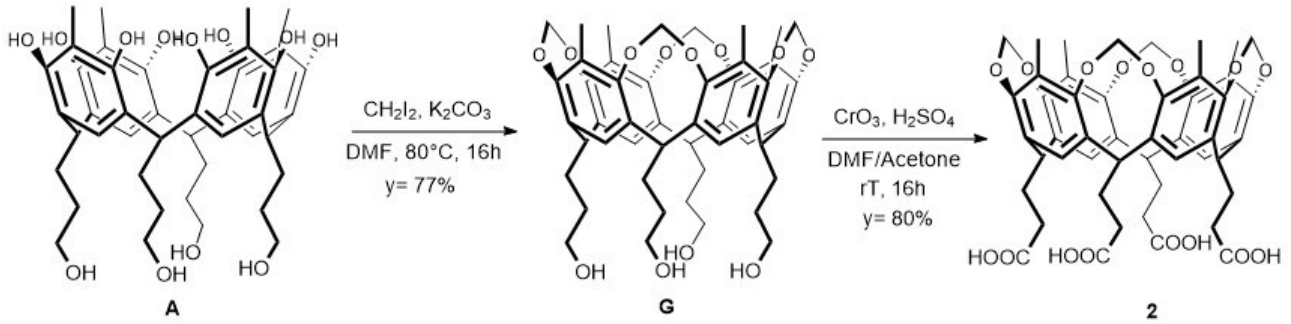

Scheme S2. Synthetic pathway for cavitand **2** preparation.

Cavitand G

Resorcinarene **A** (0.60 g, 0.77 mmol) was dissolved in 14.5 mL of anhydrous DMF. K_2CO_3 (1.07 g, 7.73 mmol) and CH_2I_2 (1.56 mL, 30.86 mmol) were added, and the solution was stirred at 80 °C for 5 hours. The reaction was cooled down to room temperature and the crude was quenched in 200 mL of water weakly acidified with HCl (37% aqueous). The obtained orange precipitate was filtered and dried to give cavitand **G** with a quantitative yield, without the need of further purification. **^{1}H NMR** (DMSO-d_6, 400 MHz): δ ppm= 7.44 (s, 4H, Ar**H**), 5.88 (d, 4H, ArOC**H_{2out}**O, J = 7.48 Hz), 4.60 (t, 4H, -C**H**-, J = 8.18 Hz), 4.47 (bs, 4H, -CH_2O**H**), 4.20 (d, 4H, ArOC**H_{2in}**O, J = 7.44 Hz), 3.50 (m, 8H, -C**H_2**OH), 2.36 (m, 8H, CHC**H_2**-), 1.90 (s, 12H, ArC**H_3**), 1.43 (m, 8H, -C**H_2**CH_2OH).**ESI-MS**: m/z 770.39 $[M+H]^+$.

Cavitand 2

To a solution of cavitand **G** (0.15 g, 0.18 mmol) in 6 mL of DMF and 6 mL of acetone, CrO_3 (0.29 g, 3.88 mmol) was added under magnetic stirring. Then, H_2SO_4 (96% aqueous) was added until pH 2 was reached and the solution was stirred at room temperature for 5 hours. The dark green solution was concentrated evaporating the solvent in high vacuum trap, then acidic water was added maintaining pH 2 and, the obtained suspension was centrifugated (10 minutes). The solid residue was washed many times with water till it reached a pale green color. The final product **2** was obtained as a pale green powder in 80% yield. **^{1}H NMR** (Acetone-d_6, 400 MHz): δ ppm = 7.60 (s, 4H, Ar**H**), 5.93 (d, 4H, ArOC**H_{2out}**O, J = 7.20 Hz), 4.86 (t, 4H, -C**H**-, J = 8.30 Hz), 4.47 (bs, 4H, -CH_2O**H**), 4.31 (d, 4H, ArOC**H_{2in}**O, J = 7.32 Hz), 2.70 (m, 8H, CHC**H_2**-), 2.36 (t, 8H, -C**H_2**COOH, J = 7.52 Hz), 1.99 (s, 12H, ArC**H_3**). **^{13}C NMR** (Acetone-d_6, 100 MHz): δ ppm = 173.79, 137.64, 124.27, 118.83, 98.57, 36.94, 31.87, 25.04, 9.41. **HR-ESI-MS**: m/z calculated for $C_{40}H_{39}O_{16}$ 823.2244 $[M-H]^-$, found 823.2247; m/z calculated for $C_{40}H_{38}O_{16}$ 411.1085 $[M-2H]^{2-}$, found 411.1085**. ATR-FTIR**: 2925 cm^{-1} C-H (aliphatic) and O-H; 1704 cm^{-1} C=O; 1428 cm^{-1} C-O-C. **TGA** (air, 25°C - 800 °C, flow rate: 20 °C/min): 8.6 % w/w loss at 117 °C; 44.7% w/w loss at 388 °C; 13.1 % w/w loss at 471 °C.

4. Ferromagnetic Nanoparticles synthesis

Synthesis of ferromagnetic nanoparticles (FeNPs)

Iron magnetite nanoparticles were synthesized by alkaline co-precipitation of Fe^{3+} and Fe^{2+}. In two separate vials, $FeCl_3 \cdot 6H_2O$ (0.73 g, 2.70 mmol) and $FeCl_2 \cdot 4H_2O$ (0.27 g, 1.36 mmol) were solubilized in 3 mL and 1.5 mL of water, respectively. In a flask, 2.2 mL of NH_3 (30% aqueous) were added to 50 mL of water and to this basic solution kept under manual stirring, the two solutions of $FeCl_3$ and $FeCl_2$ were added in quick succession. A dark colored suspension was immediately observed and left to decantation at room temperature for 2 hours. The supernatant was filtered off and the solid residue washed twice with water. The obtained FeNPs were isolated from the solvent by magnetic decantation and dried under nitrogen flux. **ATR-FTIR**: 3000 cm^{-1} OH, 551 cm^{-1} Fe-O.

Functionalized FeNPs

Functionalized FeNPs were prepared following the general protocol below.

In two different flasks, $FeCl_2 \cdot 4H_2O$ and $FeCl_3 \cdot 6H_2O$ was dissolved in water. Separately, the cavitand (see table S1 for details) was dissolved in a previously prepared solution of NH_3, DMF and H_2O. To this solution kept under manual stirring, the two Fe^{3+} and Fe^{2+} solutions were added sequentially. The formation of a dark precipitate was visible. After magnetic decantation, the supernatant was filtered off and the solid residue washed twice with water and dried under nitrogen flux.

Table S1. Reagents conditions for the preparation of functionalized FeNPs.

Sample	Cavitand solution	$FeCl_2 \cdot 4H_2O$ solution	$FeCl_3 \cdot 6H_2O$ solution
FeNPs@1	0.10 g, 0.076 mmol in 3 mL NH_3 + 8 mL DMF+ 40.8 mL H_2O	0.34 g, 1.69 mmol in 1.7 mL H_2O	0.92 g, 3.41 mmol in 3.4 mL H_2O
FeNPs@2	0.060 g, 0.068 mmol in 1.5 mL NH_3 + 30 mL H_2O	0.289 g, 1.43 mmol in 1.5 mL H_2O	0.79 g, 2.93 mmol in 3 mL H_2O

Characterization of functionalised FeNPs@1

ATR-FTIR: 3056 cm^{-1} C-H (aliphatic); 1645 cm^{-1} C=O; 1069 cm^{-1} P=O; 898 cm^{-1} O-P-O; 567 cm^{-1} Fe-O.

TGA (air, 25°C - 800 °C, flow rate: 20 °C/min): 0.1% w/w loss at 29 °C; 4.3 % w/w loss at 259 °C; 12.4% w/w loss at 388 °C.

Characterization of functionalised FeNPs@2

ATR-FTIR: 2988 cm^{-1} C-H (aliphatic); 1394 cm^{-1} C=O; 1241 cm^{-1} C-O-C; 556 cm^{-1} Fe-O.

TGA (air, 25 °C - 800 °C, flow rate: 20 °C/min): 0.6 % w/w loss at 81 °C; 13.6 % w/w loss at 298 °C.

5. ^{1}H and ^{13}C NMR characterization

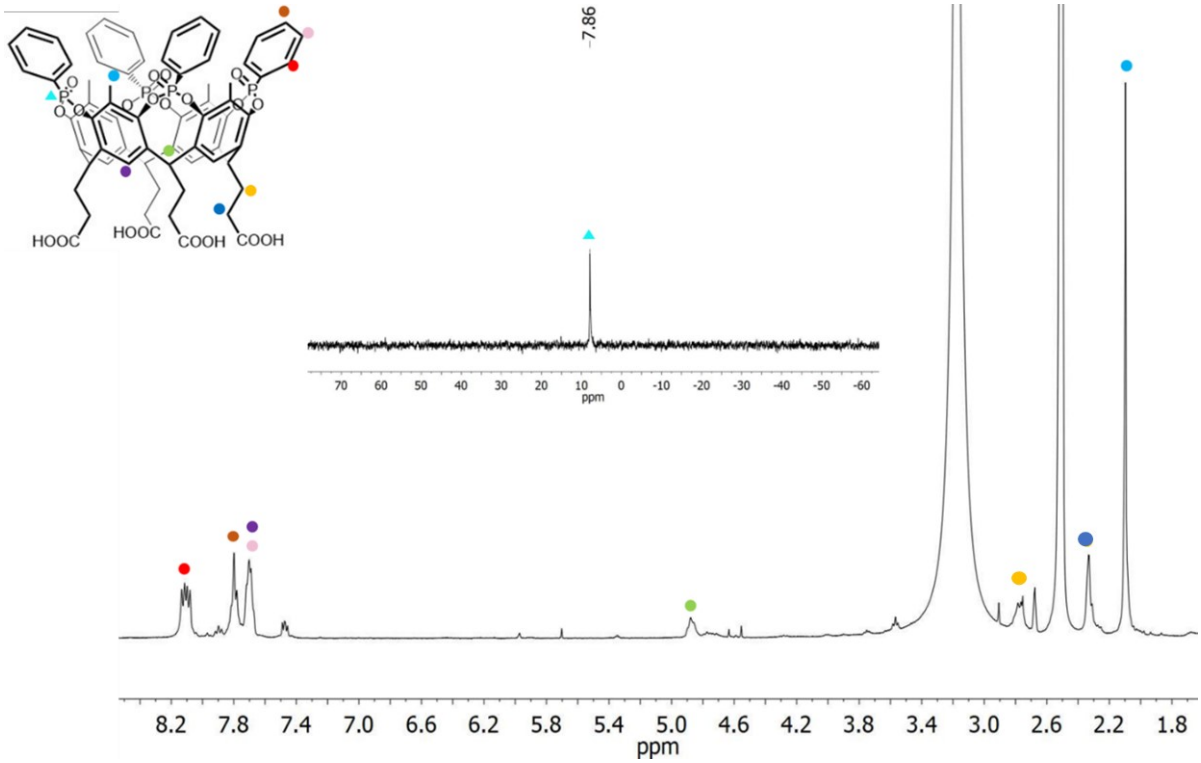

Figure S1. ^{1}H NMR of cavitand **1**, in DMSO-d_6, 400 MHz, 80 °C. Inset: ^{31}P NMR (DMSO-d_6, 162 MHz, 25°C).

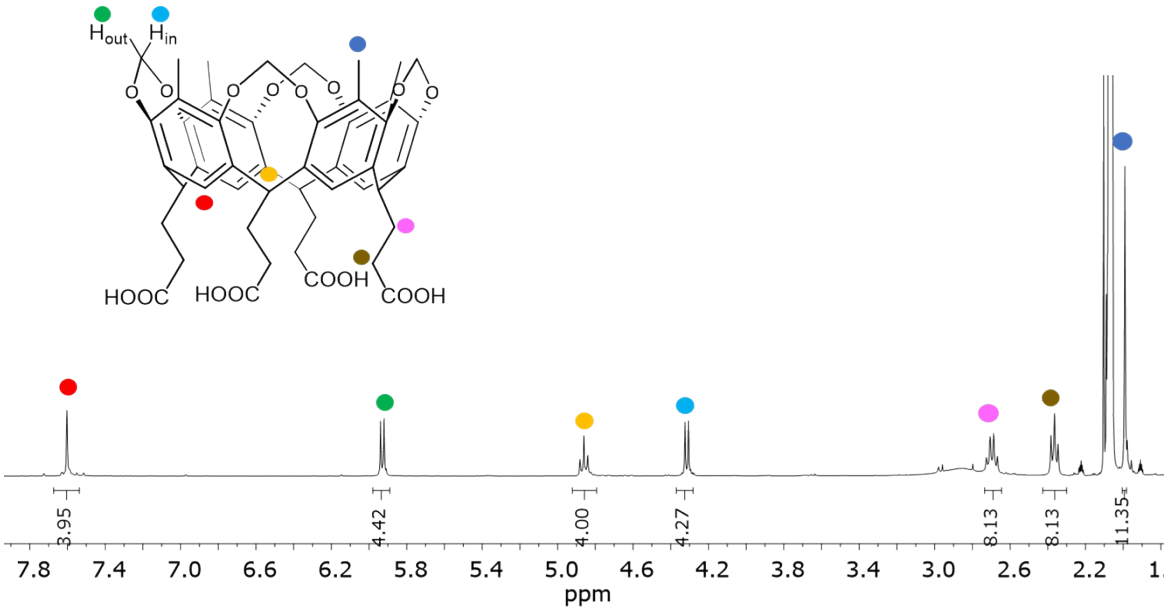

Figure S2. ^{1}H NMR of cavitand **2**, in acetone-d_6, 400 MHz, 25°C.

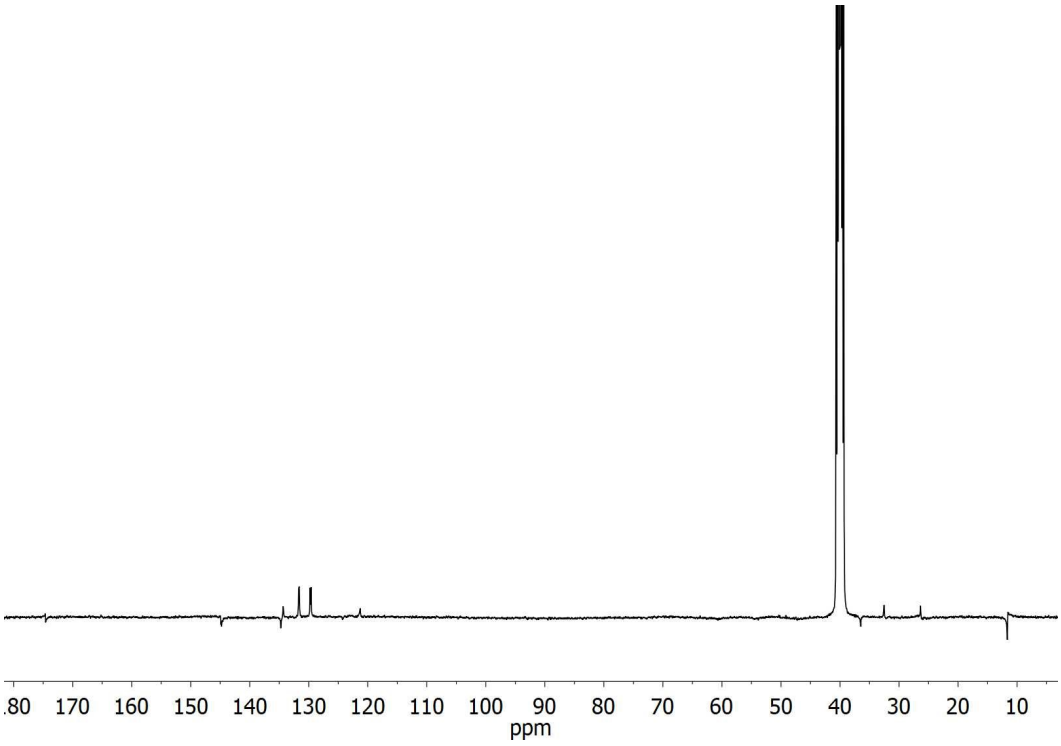

Figure S3. ^{13}C NMR of cavitand **1**, in DMSO-d_6, 100 MHz.

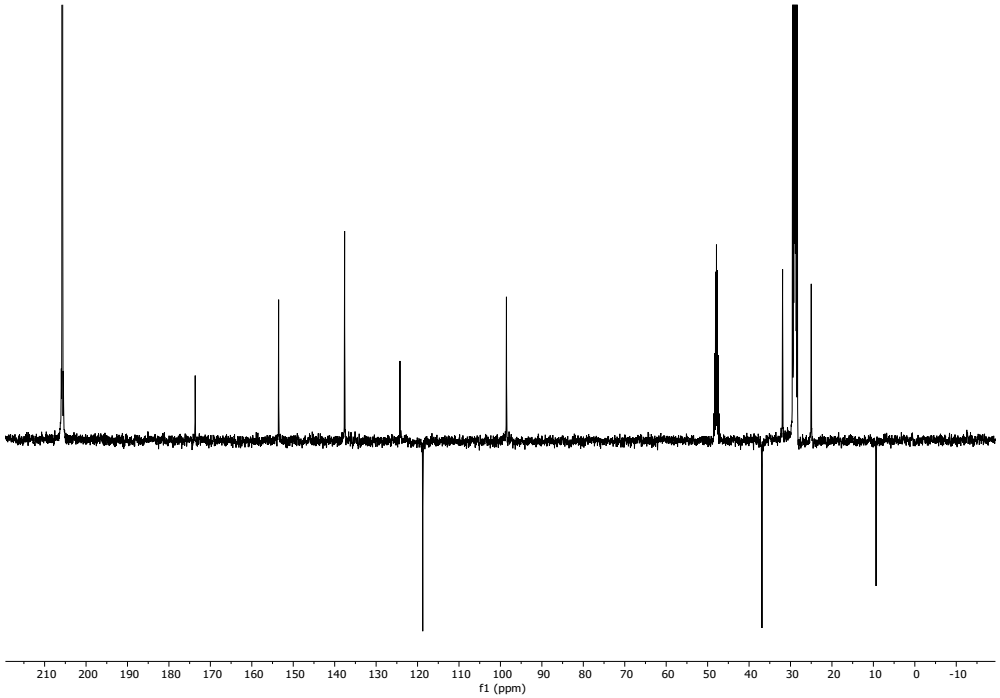

Figure S4. ^{13}C NMR of cavitand **2**, in acetone-d_6, 100 MHz, 25°C.

6. IR-ATR characterization

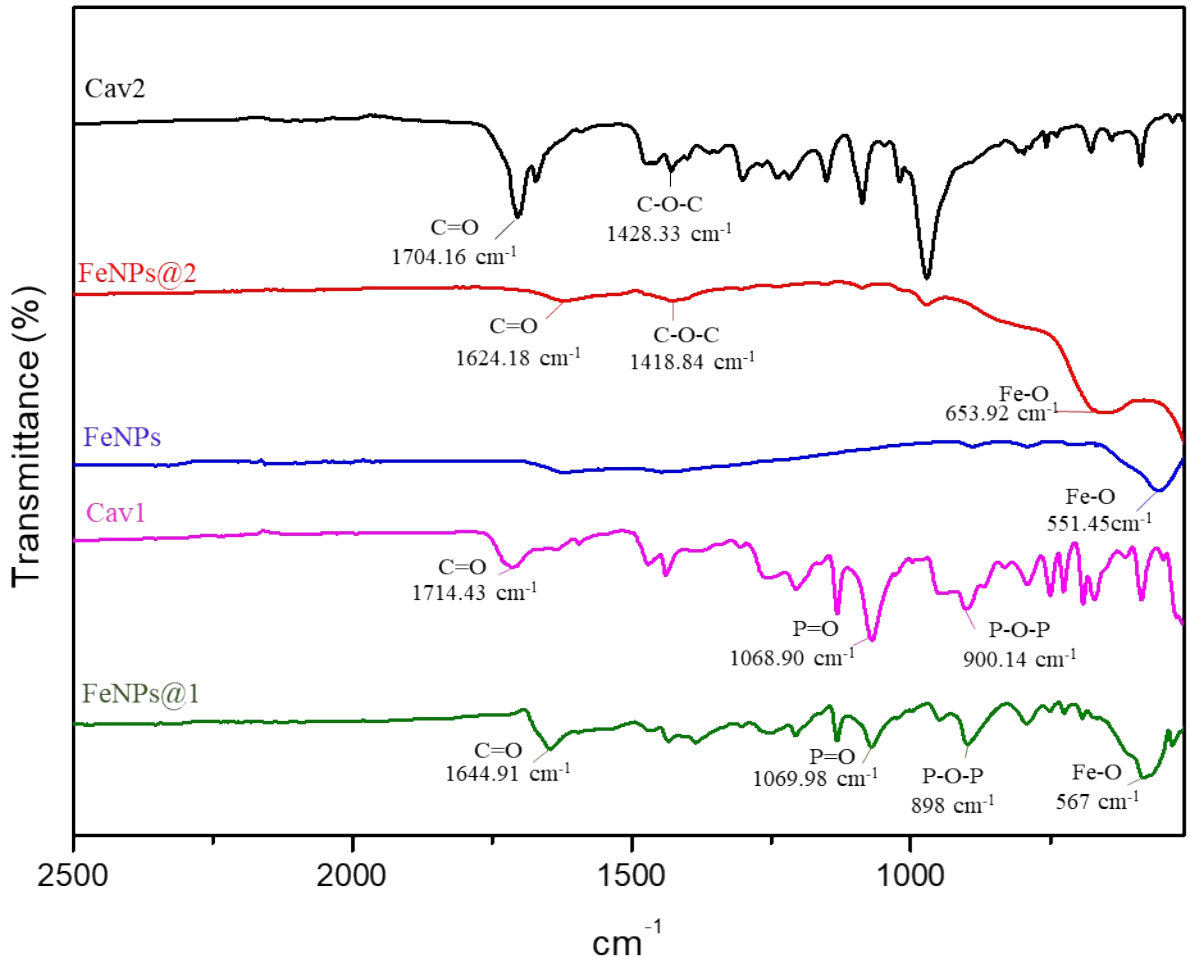

Figure S5. From bottom to top: comparison between ATR-FTIR spectra of **FeNPs@1** (green line), Cavitand **1** (magenta line), **FeNPs** (blue line), **FeNPs@2** (red line) and Cavitand **2** (black line).

7. TGA characterization

Table S2. TGA analyses results

Sample	Temperature deflection (°C)	% loss weight (first deflection)	% loss weight (second deflection)	Functionalization grade (w%)
FeNPs@1	259; 388	4.3	12.4	17
FeNPs@2	298	13.6	/	14

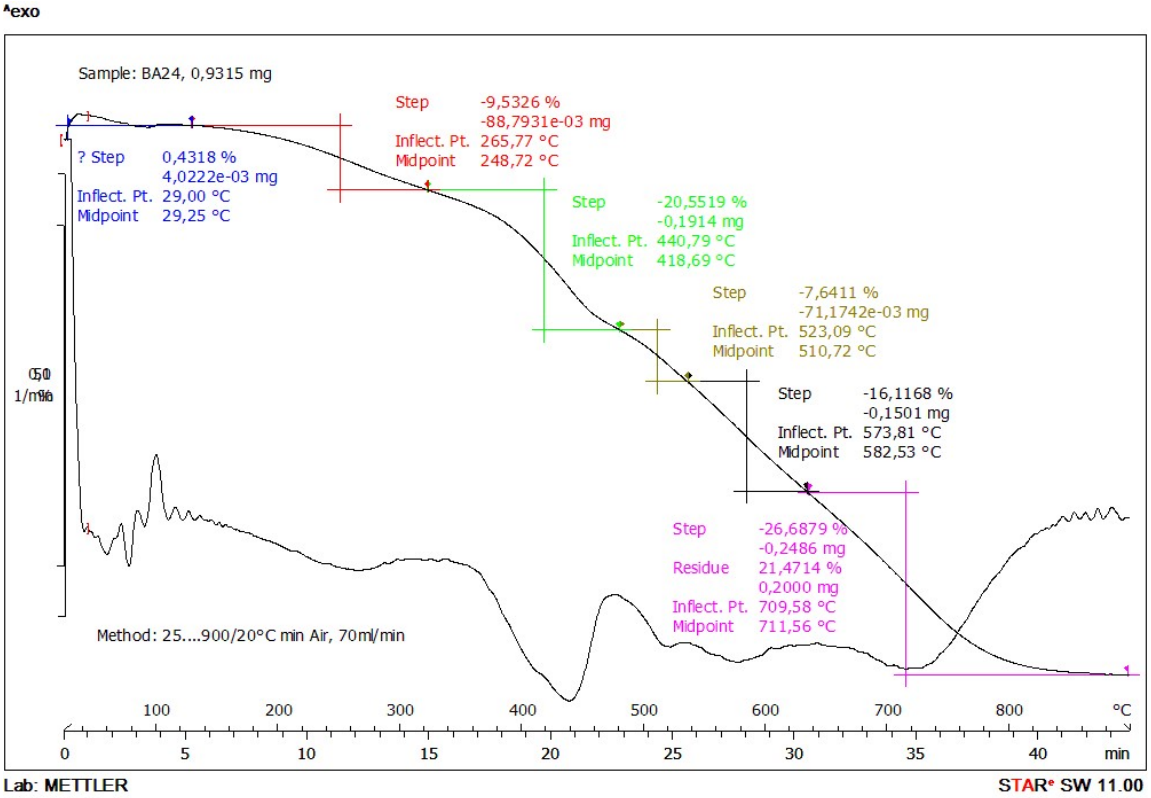

Figure S6. TGA analysis of cavitand **1**.

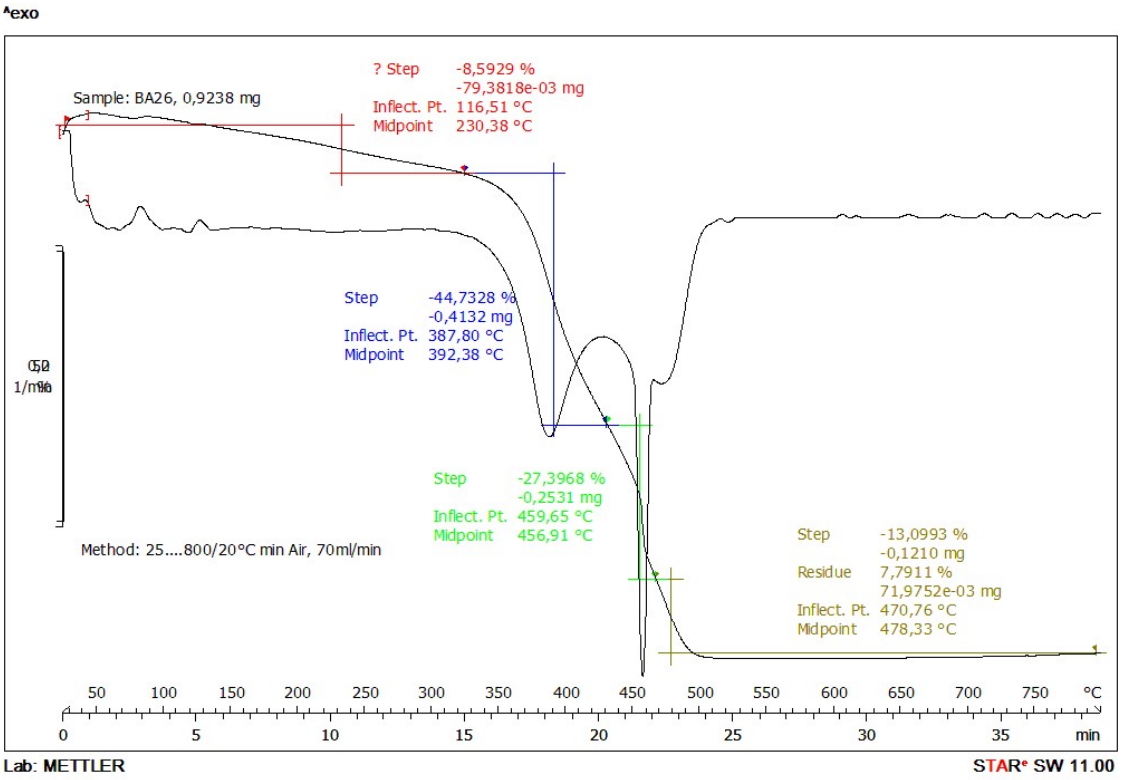

Figure S7. TGA analysis of cavitand **2**

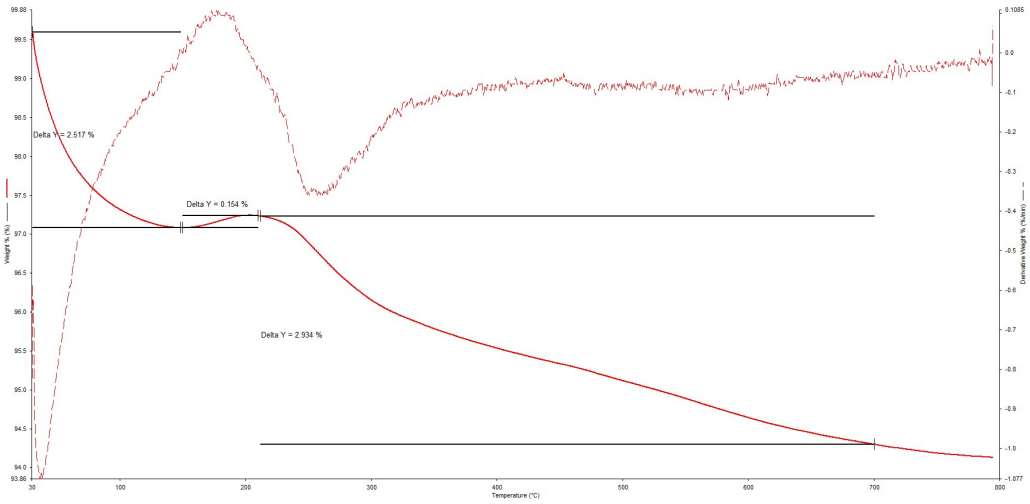

Figure S8. TGA analysis of bare FeNPs

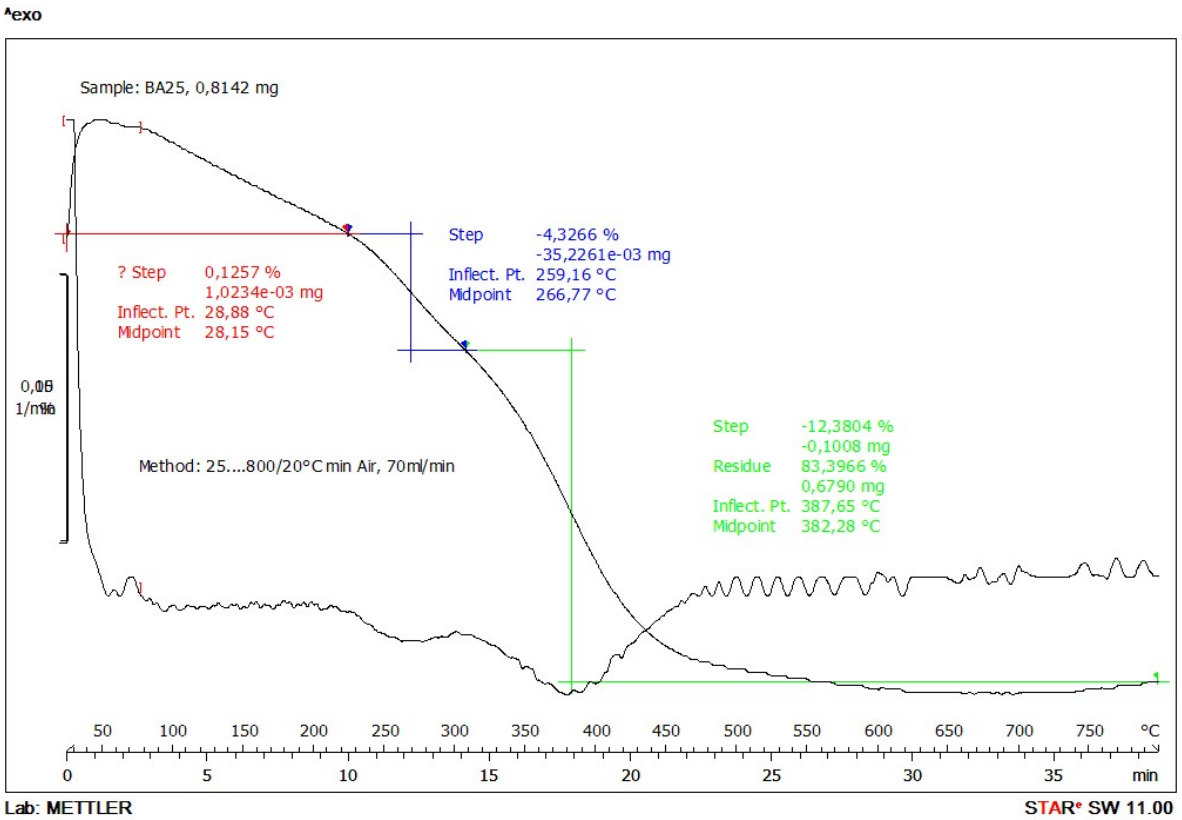

Figure S9. TGA analysis of **FeNPs@1**

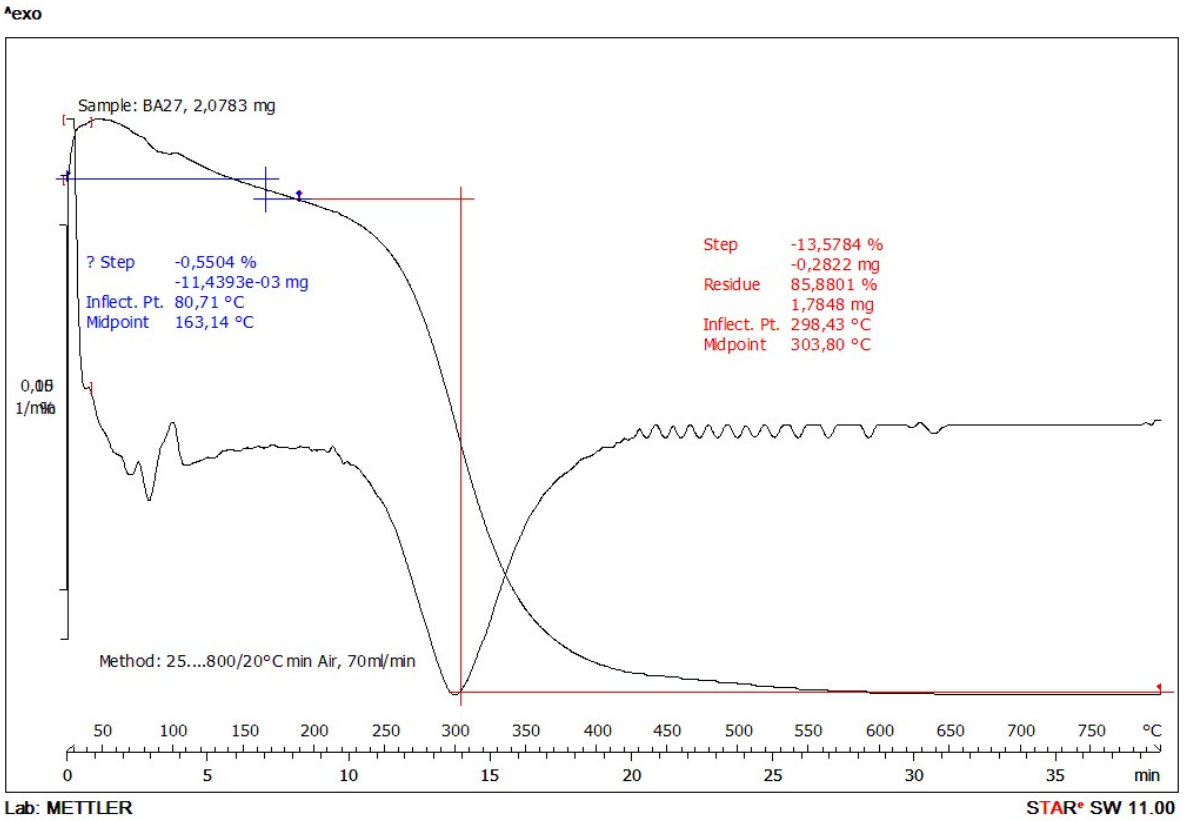

Figure S10. TGA analysis of **FeNPs@2**

8. Zeta Potential measurements

ζ potential measurements were performed for both pristine and functionalized FeNPs by preparing a suspension of nanoparticles both in water (3.5 mg in 2 mL of milliQ water, pH= 7) and basic water (3.5 mg in 2 mL of DBU solution, pH= 11). The suspension was homogenized under ultrasounds for 2 minutes before analysis.

Generally, the ζ-potential of all dispersed systems, including nanoparticles, changes as a function of the pH. In aqueous systems, Fe-OH groups covering the ferromagnetic nanoparticles surface are hydrated and their typical isoelectric point (pH where the ζ-potential is zero) is at pH ≈ 6.8.[4] Thus, below this value, the net charge for magnetite is usually positive, while above is negative. According to the literature, in neutral water, the synthesized bare FeNPs showed a positive value of ζ = 3.58 mV (Figure S11A), which can be explained by the presence of water molecules absorbed on the surface that allows the protonation of the external Fe-OH groups generating small positive charges.[5] The increase of the pH from 7 to 11 leads to the deprotonation of the hydroxyl groups, obtaining a negative value of ζ = -32.4 mV, and thus indicating a prominent anionic character of the surface (Figure S11B). The large ζ-potential value also indicates good stability of the FeNPs in water solution.

For the coated FeNPs, the ζ-potential analysis was performed at pH = 11, the same condition used for the elution experiments. In this case, a value of ζ = -35.2 and -38.7 mV was calculated for **FeNPs@1** (Figure S11C) and **FeNPs@2** (Figure S11D), respectively, slightly higher respect to the bare NPs.

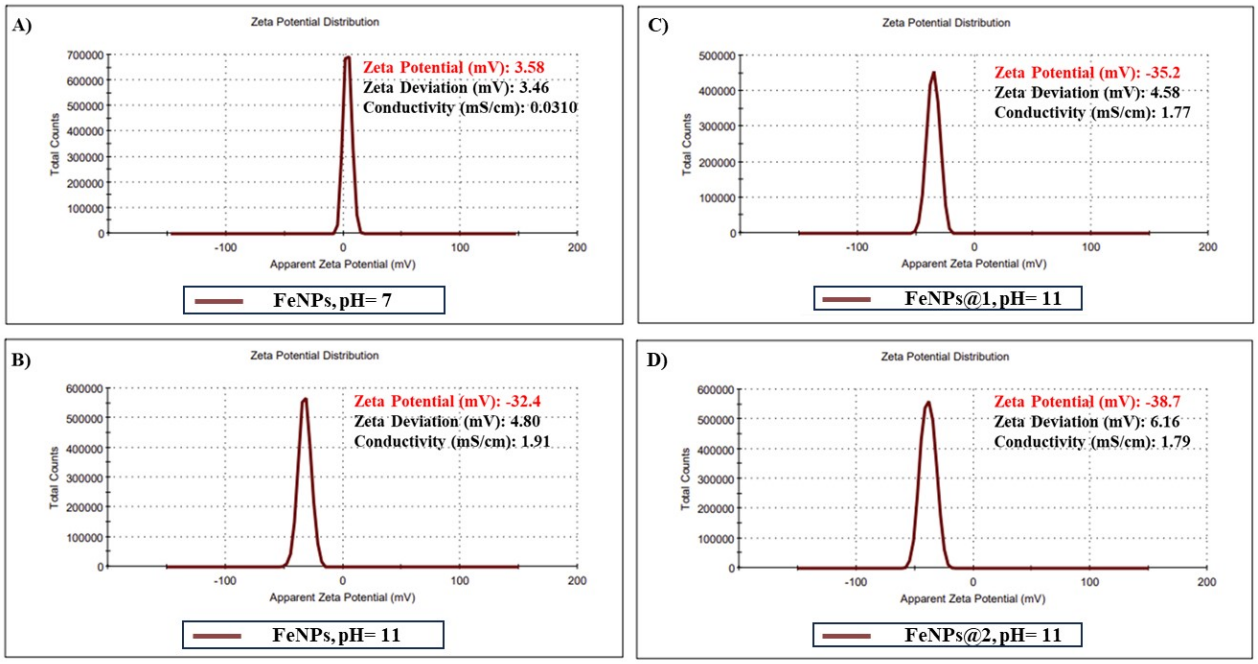

Figure S11. Zeta potential (n = 3) at room temperature of pristine **FeNPs** in A) water (pH=7) and B) basic water (pH=11), C) **FeNPs@1** in basic water (pH=11), and D) **FeNPs@2**, in basic water (pH=11).

9. X-ray Photoelectron Spectroscopy (XPS).

Bare FeNPs

XPS on iron oxide NPs showed the presence of iron, carbon, and oxygen (Figure S15). Stoichiometry analysis leads to 12%, 53%, and 35% for Fe, C, and O with a ± 3% variability in the analyzed samples (see Table S3). We found the presence of adventitious oxygen and carbon,[6,7] e.g., C-C (located at 284.97 eV), C-O (286.34 eV), C=OR (287.33 eV), and C=O (289.40 eV) in C1s and corresponding C-O/C=O contribution also in O1s core level. In the latter peak, the main contribution is located at 530.36 eV and is related to iron oxides, while peak at 530.91 eV can be due to both C=O/-OH. Fe2p core level interpretation is still a matter of debate,[8,9,10] due to the presence of a multiplet structure of core 2p vacancy levels leading to a complex line shape that is further enhanced in case of oxides. A reliable interpretation is possible using some theoretical proposed models.[11,12,13] The main peak is located at about 711 eV, a value typical for Fe_3O_4 but also for Fe^{3+} oxides (FeOOH), moreover a satellite at 718.96 eV (+8 eV from the main peak) is present and is typical of Fe^{3+} compounds but not Fe_3O_4.[12] We deconvoluted the $Fe2p_{3/2}$ peak considering the presence of both Fe^{+3} and Fe^{+2} multiplets founding a Fe^{3+}/ Fe^{2+} ratio of about 4, far from the expected 2 of Fe_3O_4 and thus confirming the presence of other Fe^{3+} species, probably FeOOH. Considering the low Fe/O stoichiometry ratio of 0.6 instead of the expected 0.75, we evaluated that about 60% of iron oxide NPs is due to Fe_3O_4 and 40% to FeOOH. Such a strange oxides combination is reflected in FeOx O1s component BE, typically in the 529.8-530.2 eV range while we observed a 530.36eV value, and in the low Fe/O ratio.

Table S3. XPS analysis results for bare **FeNPs**

Element	Chemical species	Atomic percentage (±3%)		Binding energy (eV)
		Exp.	Single species	
Fe		12		
	Fe^{3+}		9.5	711.10 (main peak)
	Fe^{2+}		2.5	709.50 (main peak)
O		35		
	FeOx		20.0	530.36
	-OH		12.0	530.91
	C-O adv.		4.0	532.20
C adv.		53		
	C-C		23.0	284.97
	C-O		16.0	286.34
	C=OR		10.0	287.33
	C=O		4.0	289.40

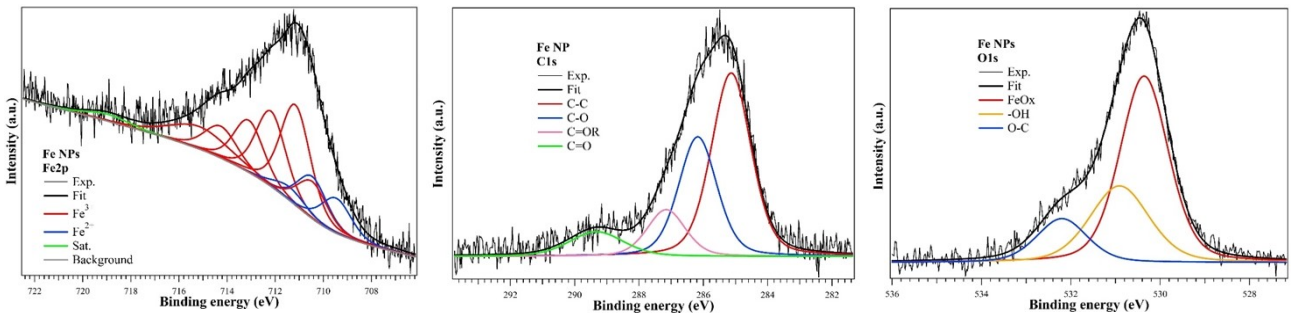

Figure S12. XPS analysis of bare **FeNPs**. Fe2p (left panel), C1s (center panel), and O1s (right panel) core levels. BEs are corrected for the shift related to the charging effects.

Cavitand 1

We found the presence of carbon (Figure S13), oxygen, and phosphorus (Figure 1, top curve) in atomic percentages of 76.2, 19.3, and 4.5%, in good agreement with the expected 74.0, 21.7, and 4.3% values. All data and peak binding energies (BEs) for cavitand **1** are shown in Table S4.

Core levels suffer a ≈+3.2 eV BE shift, due to charging during photoemission experiments (typical of insulating materials). C1s core level (Figure S13 A) reveals the presence of C-C bonds in phenyls (located at 284.74 eV, not considering the BE shift), C-C in alkyl and *meso* positions (285.31 eV), C-P (285.59 eV), C-OOH (286.29 eV).[14] The weak satellite at 288.2 eV is a shake-up transition typical of π-conjugated systems.[15] It is worth noting that the carboxyl peak shows a BE lower than expected (about 288 eV), probably due to formation of H-H bonding among some of the four alkyl chains.[16,17,18] O1s core level (Figure S13 B) is composed by four components belonging to P=O (531.61 eV), C=O (531.98 eV), O-P-O (533.22 eV), and C-OH (533.90 eV) species.[19,20] P2p core level shows a single doublet located at about 133.60 eV, in good agreement with similar organic compounds.[19,21]

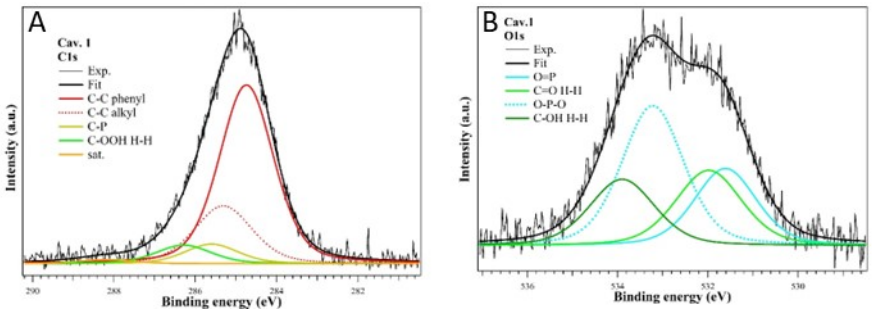

Figure S13. XPS analysis of cavitand **1**. C1s (A) and O1s (B) core levels. BEs are corrected for the shift related to the charging effects.

Table S4. XPS analysis results of cavitand **1**

Element	Chemical species	Atomic percentage		Binding energy (eV)	
		Exp. (theor.)	Single species	With shift +3.2eV	Without shift
O		19.3 (21.7)			
	P=O		4.1	534.81	531.61
	C=O H-H		4.2	535.18	531.98
	O-P-O		7.4	536.42	533.22
	C-OH H-H		3.7	537.10	533.9
C		76.2 (74.0)			
	C-C phenyl		48.3	287.94	284.74
	C-C alkyl, C-C meso		16.5	288.51	285.31
	C-P		5.2	288.79	285.59
	C-OOH H-H		5.1	289.49	286.29
	Sat.		1.1	291.40	288.2
P		4.5 (4.3)			
	P		4.5	136.88	133.68

Table S5. XPS analysis results of **FeNPs@1**. Atomic percentages values in parenthesis consider only cavitand **1** components.

Element	Chemical species	Atomic percentage		Binding energy (eV)	
		Exp. (only 1)	Single species	With shift +0.6eV	Without shift
Fe NPs		3.7			
	Fe^{3+}		3.0	711.79 (main peak)	711.19
	Fe^{2+}		0.7	709.76 (main peak)	709.16
O NPs		11.4			
	FeOx		5.8	530.31	529.71
	-OH		3.8	531.06	530.46
	C-O adv.		1.8	532.39	531.79
O cav 1		12.5 (22.2)			
	P=O		2.3	532.02	531.42
	C=O H-H		3.2	532.52	531.92
	O-P-O		4.4	533.77	533.17
	C-OH H-H		1.3	534.57	533.97
	Sat.		1.3	535.80	535.20
C NPs		28.6			
	C-C		11.0	285.76	285.16
	C-O		9.5	287.21	286.61
	C=OR		6.3	288.16	287.56
	C=O		1.8	290.16	289.56
C cav 1		41.5 (73.7)			
	C-C phenyl		26.3	285.45	284.85
	C-C alkyl, C-C meso		9.1	285.96	285.36
	C-P		2.8	286.21	285.61
	C-OOH H-H		2.7	287.03	286.43
	Sat.		0.6	289.44	288.84
P cav 1		2.3 (4.1)			
	P		2.3	134.20	133.60

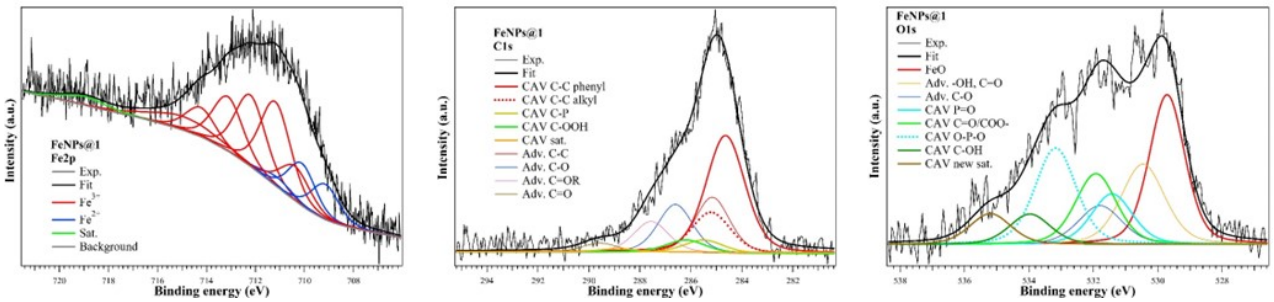

Figure S14. XPS analysis of **FeNPs@1**. Fe2p in (left panel), C1s (center panel), and O1s in (right panel) core levels. BEs are corrected for the shift related to the charging effects.

Cavitand 2

Figure S15 (top curves) shows the organic C1s and O1s core levels. Carbon, and oxygen atomic percentages are 72.4, and 27.6%, in good agreement with the expected 73.3, and 26.7% values. All data and peak binding energies (BEs) for cavitand **1** are shown in Table S6.

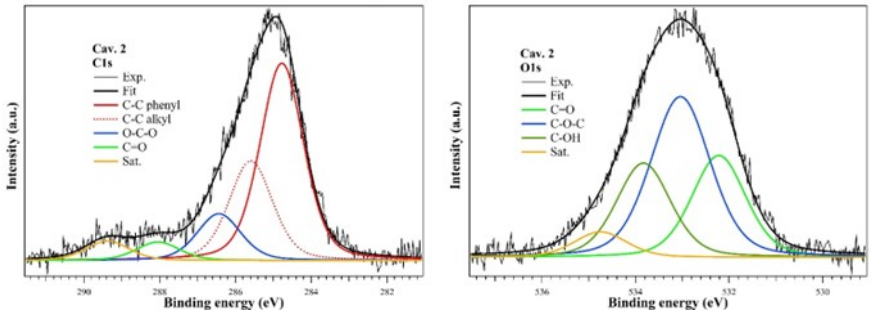

Figure S15. XPS analysis of cavitand **2**. C1s (left panel), and O1s in (right panel) core levels. BEs are corrected for the shift related to the charging effects.

Core levels suffer a ≈+2.9 eV BE shift, due to charging during photoemission experiments (typical of insulating materials). C1s core level reveals the presence of C-C bonds in phenyls (located at 284.83 eV, not considering the BE shift), C-C in alkyl and *meso* positions (285.59 eV), O-C-O (286.43 eV), C-OOH (288.04 eV).[21] The weak satellite at 289.37 eV is a shake-up transition typical of π-conjugated systems.[16] Differently from cavitand **1**, the carboxyl peak shows the correct BE, suggesting the absence for this molecule of H-H bonding formation among the four alkyl chains.[17,18,19] O1s core level is composed by four components belonging to C=O (532.21 eV), C-O-C (533.09 eV), and C-OH (533.86 eV) species,[19,21] and a weak satellite at 534.31 eV, a shake-up transition probably related to the presence of oxygen atoms in carbon based rings.

Table S6. XPS analysis results of cavitand **2**

Element	Chemical species	Atomic percentage		Binding energy (eV)	
		Exp. (theor.)	Single species	With shift +2.9eV	Without shift
O		27.6 (26.7)			
	C=O		7.0	535.11	532.21
	C-O-C		12.3	535.99	533.09
	C-OH		6.6	536.76	533.86
	Sat.		1.7	537.21	534.31
C		72.4 (73.3)			
	C-C phenyl		37.4	287.73	284.83
	C-C alkyl, C-C meso		18.9	288.49	285.59
	O-C-O		8.9	289.33	286.43
	C-OOH		3.5	290.94	288.04
	Sat.		3.7	292.27	289.37

FeNPs@2

As occurred for **FeNPs@1**, XPS analysis of **FeNPs@2** show a complex scenario. The bare **FeNPs** present a significant amount of adventitious carbon and oxygen; thus, the functionalization with the cavitand **2** will lead to the superposition of very similar photoemission peaks. We found a core level BE shift of about +2.3 eV due to charging phenomena. All data and peak binding energies (BEs) for **FeNPs@1** are shown in Table S7.

The Fe2p signal has a low S/N ratio due to the presence of the functionalizing molecules, leading to higher errors in iron core level analysis (Figure S16). Nevertheless, iron oxide properties are like bare NPs, with a slightly different multiplet structure and an increased Fe/O ratio of 0.68, instead of 0.54. The C1s (Figure S16) and O1s (Figure S16) core levels can be reliably reproduced as the superposition of components from the inorganic adventitious species and the organic features, i.e., the cavitand **2** is present on the **FeNPs**; however, a detailed comprehension is not fully reliable. The relative atomic percentages of the cavitand contribution for C, and O are 79.8, and 20.2%, in fair agreement with previous results (see Table S6). C1s core level shows the same components of the isolated cavitand, with only the COOH group (287.19 eV) at a -0.9 eV BE and a significant decrease in intensity. O1s core level analysis revealed a shift to higher BE of C=O and COH peaks (about +0.3 eV) and a different intensity ratio, with the former being more intense. These results suggest the interaction of COOH groups with **FeNPs**, as occurred for **FeNPs@1**.[22] We can conclude that functionalization occurs *via* the organic carboxyl groups.

Table S7. XPS analysis results of **FeNPs@2**. Atomic percentages values in parenthesis consider only cavitand **2** components.

Element	Chemical species	Atomic percentage (±2%)		Binding energy (eV), shift +2.3eV	
		Exp.	Single species	With shift +2.3eV	Without shift
Fe NPs		9.1			
	Fe^{3+}		5.4	713.72 (main peak)	711.42
	Fe^{2+}		3.7	711.92 (main peak)	709.62
O NPs		15.4			
	FeOx		13.3	533.91	531.61
	-OH		2.1	534.81	532.51
	C-O adv.		-		
O cav 2		11.5			
	C=O		3.5	534.76	532.46
	C-O-C		5.7	535.58	533.28
	C-OH		2.3	536.64	534.34
	Sat.		-	-	-
C NPs		18.5			
	C-C		11.1	287.95	285.65
	C-O		5.3	289.10	286.80
	C=OR		2.1	290.60	288.30
	C=O		-	-	
C cav 2		45.5			
	C-C phenyl		23.5	287.12	284.82
	C-C alkyl, C-C meso		10.6	287.91	285.61
	O-C-O		5.6	288.74	286.44
	COO-		1.9	289.49	287.19
	C=O		1.6	290.44	288.14
	Sat.		2.3	291.59	289.29

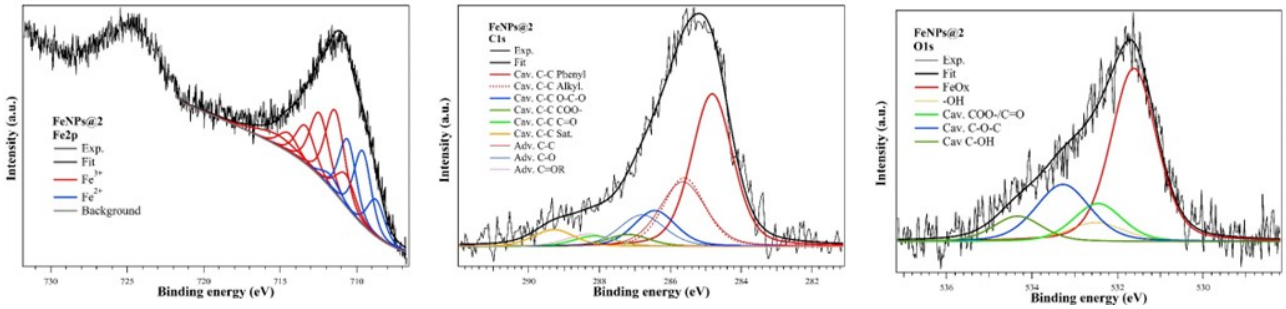

Figure S16. XPS analysis of **FeNPs@2**. Fe2p in (left panel), C1s (center panel), and O1s in (right panel) core levels. BEs are corrected for the shift related to the charging effects.

10. XRD characterization

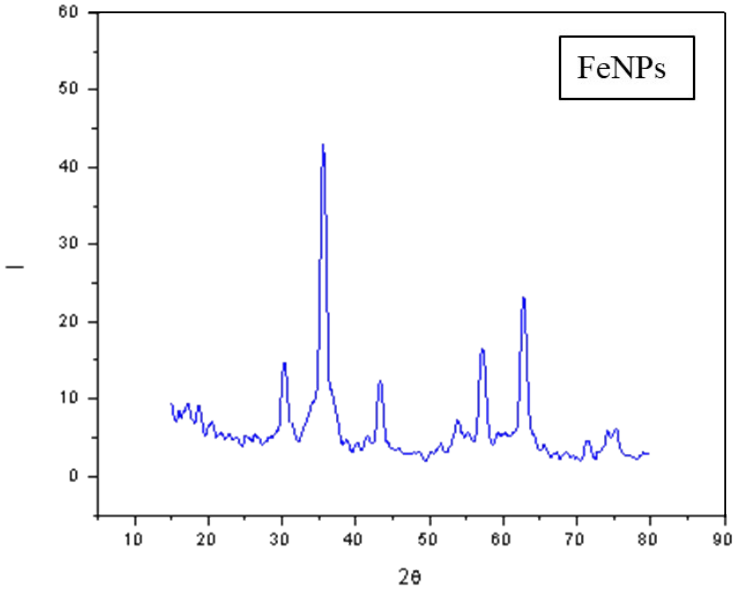

Figure S17. XRD pattern of bare **FeNPs**

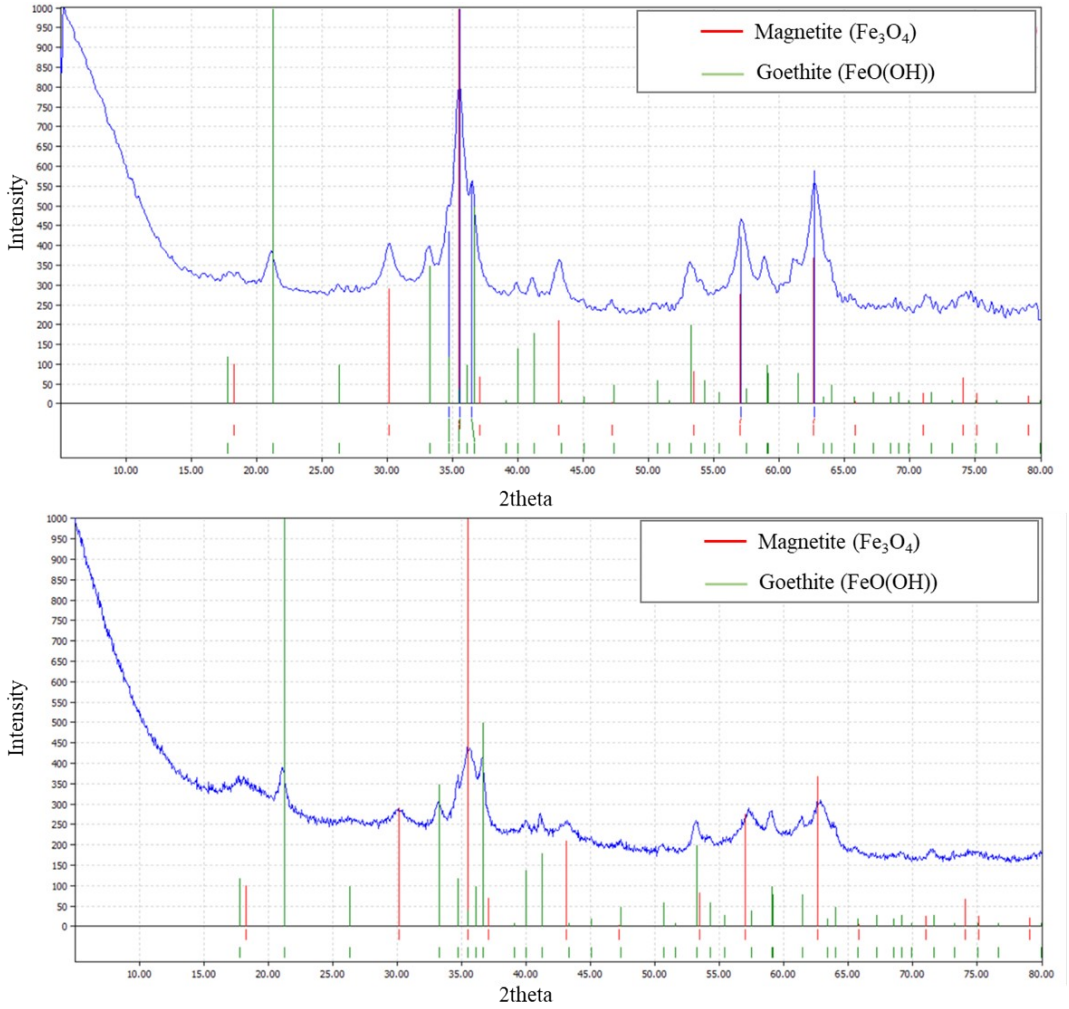

Figure S18. XRD patterns of **FeNPs@1** (*top*) and **FeNPs@2** (*bottom*).

11. Transmission Electron Microscopy

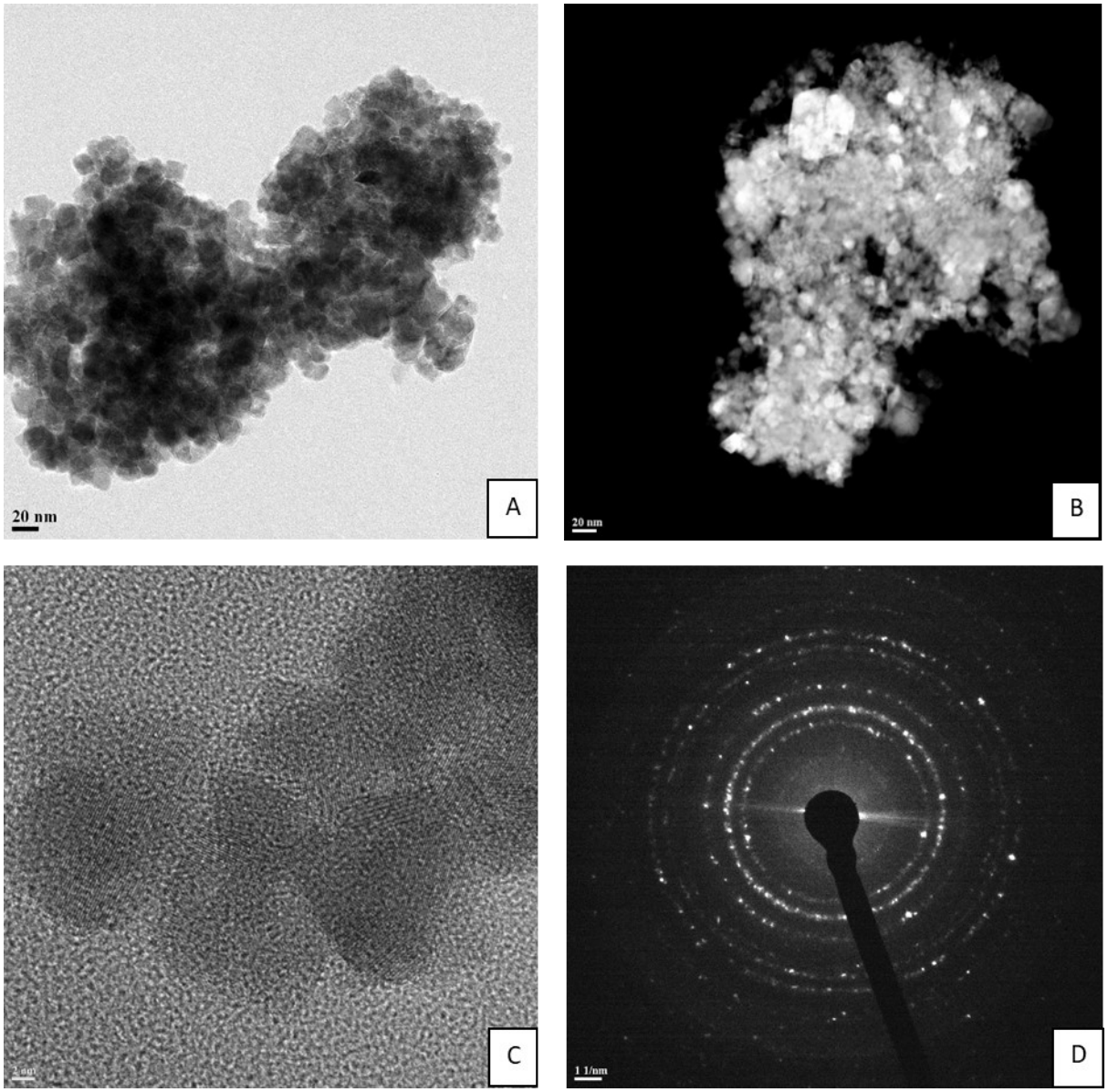

Figure S19. Images of: TEM (**A**), STEM (**B**), and HR-TEM (**C**) of bare FeNPs. In (**D**) the Diffraction Pattern collected in the region of picture in (**B**), confirms the phase is magnetite.

12. Proteolytic digestion protocol

The proteolytic digestion was performed using Arg-C (clostripain), an endopeptidase that cleaves at the C-terminus of arginine residues, as well as occasionally after lysine residue (1-4). This sequencing-grade enzyme is commonly used for protein analysis by mass spectrometry. We used Arg-C because this enzyme cleaves only at the arginine residues. This allows for the generation of peptides containing multiple lysine residues, enabling us to take advantage of multivalency.

During the proteolytic digestion, the histone proteins were solubilized in an aqueous incubation buffer (pH= 7.8). Arg-C, suspended in the same buffer, was then added. After incubation at 37°C for 14.5 hours, the obtained digested histones were heated at 95 °C for 10 minutes to quench the reaction. The sample was then lyophilized and stored at -20°C. The buffer was prepared as follows:

- TRIS-HCl buffer: 4.01 mL, final concentration: 50 mM
- $CaCl_2$: 2.78 mg, final concentration 5 mM
- EDTA: 2.92 mg, final concentration 2 mM
- DTT (dithiothreitol): 3.86 mg, final concentration 5 mM

The protocol is based on 4 steps:

- 500 µg of histones (from calf thymus, Type II-A, lyophilized powder) were solubilized in 0.5 mL of water-based incubation buffer (pH=8).
- 10 µg of commercial Arg-C enzyme were suspended in 20 µL of incubation buffer and added to the previous solution.
- The system was heated at 37 °C for 14.5 hours using a thermal cyclator (100 rpm).
- The digestion was quenched heating the system at 95 °C for 10 minutes.

For the enrichment experiment we used in total 1.5 mg of histones divided in 3 batch of

13. Enrichment protocol

The tests were carried out as following:

- The FeNPs were dissolved in 60 µL of Milli-Q water (used quantities: 4.5 mg of bare **NPs**, 6.8 mg **FeNPs@1** and 4.5 mg of **FeNPs@2**).
- 10 µL of the Milli-Q water solution containing the digested histones were added. This solution was prepared digesting 1.5 mg of histones and then dissolving the lyophilized obtained peptides in 520 µL of Milli-Q water.

For each batch, 5 replicates were produced to prove reproducibility. The protocol is depicted in Figure 3A.

- 100 µL of a water solution of DBU (pH 12.2), was added to the FeNPs recovered from the incubation step.
- The obtained mixture was stirred using a vortex mixer for 2 h.
- The FeNPs were let to precipitate with the help of a magnet and the supernatant was removed. The procedure was repeated twice.
- The collected supernatants were lyophilized and analyzed by LC-MS/MS analysis.

14. Immunoprecipitation protocol

The IP experiment was carried out adapting the protocol provided from PTMScan® Technology (Figure 4A, main text). 5 replicates were performed to prove reproducibility.

- In a 2 mL Eppendorf tube, 10 µL of Milli-Q water solution of the digested histones proteins were diluted with 1.4 mL of IAP Buffer (composed by 50% glycerol and provided by PTMScan® Technology).
- The solution was centrifuged (5 minutes, 10,000 g, 4°C) and kept in ice bath.
- The commercial antibody beads were discarded from their provided supernatant by centrifuging the tube (2,000 g) for 30 seconds then, washed with 1 mL of PBS buffer solution, and resuspended in 40 µL of PBS buffer.

- The peptide solution was added to the antibody beads tube and let in incubation for 2h, at 4°C, keeping the system under rotation using a Revolver Rotator, Labnet (100 rpm).
- The supernatant was discarded, and the beads were washed two times with 1 mL of IAP buffer and three times with 1 mL of Milli-Q water, centrifuging the system after each washing step (30 seconds, 2,000 g, 4°C).
- 55 µL of a 0.15 % aqueous solution of TFA was added to the beads and the system was let stand at room temperature for 10 minutes, mixing the tube after every 2-3 minutes by tapping gently the bottom of the Eppendorf several times. This step was repeated twice.
- The supernatants were collected in a new Eppendorf tube, lyophilized and analyzed via LC-MS/MS analysis.

15. Sample preparation for LC-MS/MS analysis

Sample desalting

Prior to mass spectrometry analysis, samples were desalted using a 96-well plate filter (Orochem) packed with 1 mg of Oasis HLB C-18 resin (Waters). Briefly, the samples were resuspended in 100 µl of 0.1% TFA and loaded onto the HLB resin, which was previously equilibrated using 100 µl of the same buffer. After washing with 100 µl of 0.1% TFA, the samples were eluted with a buffer containing 70 µl of 60% acetonitrile and 0.1% TFA and then dried in a vacuum centrifuge.

LC-MS/MS Acquisition and Analysis

Samples were resuspended in 10 µl of 0.1% TFA and loaded onto a Dionex RSLC Ultimate 300 (Thermo Scientific), coupled online with an Orbitrap Fusion Lumos (Thermo Scientific). Chromatographic separation was performed with a two-column system, consisting of a C-18 trap cartridge (300 µm ID, 5 mm length) and a picofrit analytical column (75 µm ID, 25 cm length) packed in-house with reversed-phase Repro-Sil Pur C18-AQ 3 µm resin. Peptides were separated using a 30 min gradient from 4-30% buffer B (buffer A: 0.1% formic acid, buffer B: 80% acetonitrile + 0.1% formic acid) at a flow rate of 300 nl/min. The mass spectrometer was set to acquire spectra in a data-dependent acquisition (DDA) mode. Briefly, the full MS scan was set to 300-1200 m/z in the orbitrap with a resolution of 120,000 (at 200 m/z) and an AGC target of 5x10e5. MS/MS was performed in the ion trap using the top speed mode (2 secs), an AGC target of 1x10e4 and an HCD collision energy of 35. Proteome raw files were searched using Proteome Discoverer software (v2.5, Thermo Scientific) using SEQUEST search engine and the bovine histone SwissProt database. The search for total proteome included variable modification of mono- and di-methylation on lysine and arginine residues, and tri-methylation on lysine residues. ArgC was specified as the digestive enzyme with up to 2 missed cleavages allowed, and it was set as semi-specific due to the imprecision of the enzyme in digesting exclusively after arginine residues (PMID: 1652592).[23] Mass tolerance was set to 10 pm for precursor ions and 0.2 Da for product ions. Peptide and protein false discovery rate was set to 1%. Following the search, data were imported into Skyline[1] to extract the ion chromatogram of the (un)modified peptides. Specifically, we exported the area under the curve of the precursor ion according to Skyline. We then calculated enrichment ratios between the enriched fraction and the supernatant (see main text, Figure 3A).

16. References

1. Williams, D. B. G., Lawton, M. J. *J. Org. Chem.* 2010, **75**, 8351–8354.
2. MacLean, B., Tomazela, D. M., Shulman, N., Chambers, M., Finney, G. L., Frewen, B., Kern, R., Tabb, D. L., Liebler, D. C., and MacCoss, M. J. *Bioinformatics* 2010, **26**, 966–968.
3. Yuan, Z.-F., Sidoli, S., Marchione, D. M., Simithy, J., Janssen, K. A., Szurgot, M. R., and Garcia, B. A. *J. Proteome Res.* 2018, **17**, 2533–2541.
4. Villegas, V. A. R., De León Ramírez, J. I., Guevara, E. H., Sicairos, S. P., Ayala, L. A. H., and Sanchez, B. L. *J. Saudi Chem. Soc.* 2020, **24**, 223–235.
5. Vasić, K., Knez, Ž., Konstantinova, E., Kokorin, A., Gyergyek, S., and Leitgeb, M. K. *React. Funct. Polym.* 2020, **148**, 104481.
6. Yamashita, T., Hayes, P. *Appl. Surf. Sci.* 2008, **254**, 2441–2449.
7. Zubir, N. A., Yacou, C., Motuzas, J., Zhang, X., and Diniz Da Costa, J. C. *Sci. Rep.* 2014, **4**, 1–8.
8. Parkinson, G. S. *Surf. Sci. Rep.* 2016, **7**, 272–365.
9. Yamashita, T., Hayes, P. *J. Electron Spectros. Relat. Phenomena* 2006, **152**, 6–11.
10. Paparazzo, E. J. Electron Spectros. Relat. Phenomena 2006, **154**, 38–40.
11. Gupta, R. P., Sen, S. K. *Phys. Rev. B.* 1975, **12**, 15–19.
12. Grosvenor, A. P., Kobe, B. A., Biesinger, M. C., and McIntyre, N. S. *Surf. Interface Anal.* 2004, **36**, 1564–1574.
13. Biesinger, M. C., Payne, B. P., Grosvenor, A. P., Lau, L. W. M., Gerson, A. R., and Smart, R. S. C. *Appl. Surf. Sci.* 2011, **257**, 2717–2730.
14. Briggs, D., Beamson, G. *Anal. Chem.* 1992, **64**, 1729–1736.
15. Bidermane, I., Lüder, J., Boudet, S., Zhang, T., Ahmadi, S., Grazioli, C., Bouvet, M., Rusz, J., Sanyal, B., Eriksson, O., Brena, B., Puglia, C., and Witkowski, N. *J. Chem. Phys.* 2013, **138**, 234701.
16. Garcia-Gil, S., Arnau, A., and Garcia-Lekue, A. *Surf. Sci.* 2013, **613**, 102–107.
17. Liu, Y., Xu, Z., Zhang, J., Cheng, J., Miao, M., and Zhang, D. *Dyes Pigment* 2019, **170**, 107586.
18. Pantano, M. F., Tatti, R., Aversa, L., Verucchi, R., and Pugno, N. M. *Front. Mater.* 2020, **7**, 197.
19. Luo, W., Zemlyanov, D. Y., Milligan, C. A., Du, Y., Yang, L., Wu, Y., and Ye, P. D. *Nanotechnology* 2016, **27**, 434002.
20. Briggs, D., Beamson, G. *Anal. Chem.* 1993, **65**, 1517–1523.
21. Ghiami, A., Timpel, M., Nardi, M. V., Chiappini, A., Nozar, P., Quaranta, A., and Verucchi, R. *J. Phys. Chem. C* 2020, **124**, 6732–6740.
22. Nardi, M. V., Timpel, M., Pasquardini, L., Toccoli, T., Scarpa, M., and Verucchi, R. *Materials* 2023, **16**, 5390.
23. Krueger, R.J, Hobbs, T. R., Mihal, K. A., Tehrani, J., and Zeece, M. G. *J Chromatogr.* 1991, **543**, 451-461.